Theoretical Study of Wetting Behavior of Nanoparticles at Fluid Interfaces

Jianguo Mi, Yongjin He, and Chongli Zhong
Laboratory of Computational Chemistry, Dept. of Chemical Engineering,
Beijing University of Chemical Technology, Beijing 100029, China

DOI 10.1002/aic.11694
Published online January 22, 2009 in Wiley InterScience (www.interscience.wiley.com).

In this work, a theoretical model was developed to describe the wetting behavior of nanoparticles at liquid-vapor interface by the integration of the renormalization group transformation, the cell theory, and the modified fundamental measurement theory with the first-order mean spherical approximation method. The results show that the new model can be used to investigate the global behavior and surface tensions of nanoparticle/fluid systems. Particularly, the nanoparticle's wetting behavior inside critical region was discussed systematically. More important, this work proposed a methodology for calculating line tension and contact angle, showing that line tension has considerable influence on wetting properties for small nanoparticles, whereas it is negligible for large nanoparticles. Therefore, this work provides a general method for studying the wetting behavior of nanoparticles that may find wide applications in the field of chemical engineering. © 2009 American Institute of Chemical Engineers *AIChE J,* 55: 747–755, 2009

Keywords: global phase equilibria, surface tension, line tension, contact angle, wetting

Introduction

Nanoparticles adsorbed at fluid interface are of practical interest in various applications such as emulsions, foams, dispersions, adsorption-based separations, and heterogeneous chemical reactions.[1,2] Because of small size, their properties depart significantly from those of macroscopic materials.[3] Unlike the wetting phenomena at the macroscopic scale that have been well understood,[4–6] spreading of a liquid on a small nanoparticle involves a complex behavior in the vicinity of vapor, liquid, and particle three-phase contact region. The contact line is the frontier between the vapor-liquid, vapor-particle, and liquid-particle interfaces. The description of wetting requires accounting for not only the interfacial surface properties but also the special properties of the triple line. The line tension, a characteristic property of three-phase interactions, has to be considered generally.

The determination of line tension has an important engineering impact, such as in the separation of crushed minerals by floatation,[7] dispersion of colloidal nanoparticles in liquid film in the petrochemical industry,[8] and the attachment/detachment of metallic or semiconducting nanoparticles to change their optical or electronic properties from liquid drops or bubbles.[9] In these systems, the variation of ionic strength and the nanoparticle size induces large changes in the interfacial tension and line tension, resulting in different interface properties of fluid-nanoparticle systems. A review on the experimental determination of line tension as well as its relation to engineering can be found in Ref. 10.

However, the accurate experimental measurement of the line tension is still a big challenge to date. Most of these experiments are based on microparticles, and many rely on optical microscopes to deduce the contact angle from geometric measurements.[3] There are obvious limitations to extend these methods to nanoparticles; line tensions inferred from experiments span several orders of magnitude, reflecting the difficulty of experimental techniques. On the other hand, computer simulations have proved helpful in extending our understanding of the mechanisms of three-phase interactions. Using molecular dynamics simulations, Bresme and Quirke[11–13] obtained the line tensions by the excess free energy calculations. The line tensions can be both positive

Correspondence concerning this article should be addressed to C. Zhong at zhongcl@mail.buct.edu.cn or zhongcl88@yahoo.com.

© 2009 American Institute of Chemical Engineers

and negative, depending on the particle size and the interfacial tension of the fluid interfaces. In addition to quantifying the nanoparticle line tension, they provided a molecular view of the three phase line and enabled testing the validity of the Young's and the modified Young's equations[6] for nanoparticles at fluid interfaces. In their works, they found that the two approaches are consistent for large nanoparticles; whereas for small nanoparticles, obvious difference always exists between the two methods[11]; the difference is due simply to the line tension contribution. These works indicate that an accurate line tension description of the system by molecular simulation is not easy.

Thermodynamic theory provides an alternative way to give a comprehensive interpretation of line tensions. Marmur and coworkers[14,15] analyzed the energy associated with line tension for a vapor-liquid-particle system and defined it as the difference between the actual interfacial energy of the system and the sum of the interfacial energies of the individual interfaces. An approximate equation was constructed to deal with the line tension as well as the contact angle of liquid drops on nanospheres. Recently, Widom and coworkers[16,17] provided a geometric interpretation of adsorption at the three-phase contact line, and conjectured a line adsorption equation. Very recently, Schimmele and Napiórkowski[18] analyzed a droplet in contact with a gas on a solid substrate systematically. They found two different possible definitions of the line tension: one is independent of the choice of the Gibbs dividing interfaces, and the other is opposite. These works show that for nanoparticles at fluid interface, the line tension and curvature effects on the interfacial surface tension have to be considered simultaneously, and the surface tension of curvature expansion has to be known in advance before the line tension could be determined.

A curved surface presents several fundamental differences with a planar surface. Wetting of planar surface has been investigated systematically, and the validity of the Young's equation for describing the wetting behavior of a fluid adsorbed on a planar substrate has been tested.[19–21] While for curved surfaces, the magnitude of the surface tension as well as the order of wetting and drying transitions are affected by the curvature[2,22]; such curvature dependence of the surface tension can be characterized by Tolman length,[23] which has been discussed in our previous work[24] for a spherical particle in contact with fluids.

In this work, we try to establish a general model based on the statistical mechanics to describe the wetting behavior of nanoparticles at the vapor-liquid interface, in which the calculation of line tension will be intensively discussed. We develop the theory with a nonlocal density functional method, where the modified fundamental measurement theory (MFMT),[25,26] the first-order mean spherical approximation (FMSA),[27–31] and the renormalization group (RG) transformation[32–34] for the critical phenomena are incorporated. Apart from a systematic description of global phase behavior and surface tension, the present theory also gives the first estimate of the line tension as well as the modified contact angle of nanoparticles at fluid interface. In addition, our model can be used to discuss the wetting behavior at temperature near the critical point.

The article is organized as follows: in the part of theory, we presented the details to predict the global vapor-liquid-solid phase equilibria for Lennard-Jones/spline (LJ/s) fluids, in which a model was developed by combining the FMSA, the RG transform, and the cell model[35,36]; in the result and discussion part, we presented the results for global phase diagram, fluid structure, vapor-nanoprticle, and liquid-nanoparticle surface tensions, as well as the contact angles both by the Young's and modified Young's equations; conclusions were given in the final part.

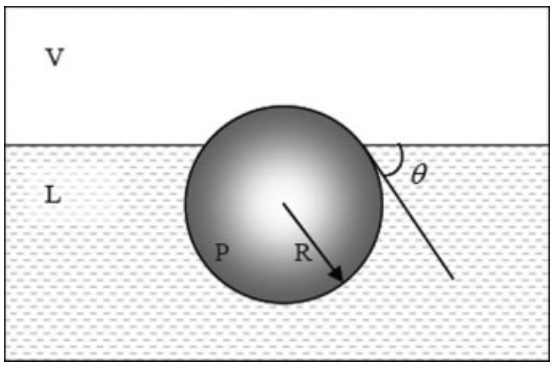

Figure 1. Illustration of a particle at the vapor-liquid interface.

Theory

The problem considered here is the nanoparticle of radius R at a planar liquid-vapor interface. The location of the particle can be described in terms of contact angle θ, as shown in Figure 1. The contact angle can be valued from 0 to 180, corresponding to wetting and drying, respectively.

Potential model

To compare our theoretical calculation with the available molecular simulation data, we adopt the same potential model to describe the interactions of the system as in molecular simulations, which is based on the Lennard-Jones/spline potential[37]

$$u_{ij}(r) = \begin{cases} 4\varepsilon_{ij}\left[\left(\frac{\sigma_f}{r-s}\right)^{12} - \left(\frac{\sigma_f}{r-s}\right)^{6}\right] & 0 < r-s < r_{s,ij} \\ a_{ij}\left(r-s-r_{c,ij}\right)^2 + b_{ij}\left(r-s-r_{c,ij}\right)^3 & r_{s,ij} < r-s < r_{c,ij} \\ 0 & r_{c,ij} < r-s \end{cases} \quad (1)$$

where r is the distance between particles, σ_f is the diameter of the fluid particles, ε_{ij} represents the potential depth for interaction between species i and j, and $s = (\sigma_p - \sigma_f)/2$, the subscript "p" and "f" represent the particle and fluid respectively, in which $\sigma_p = 2R$ is the diameter of the particulate. The remaining variables are given by $r_{s,ij} = (26/7)^{1/6}\sigma_f$, $r_{c,ij} = (67/48)r_{s,ij}$, $a_{ij} = -(24192/3211)(\varepsilon_{ij}/r_{s,ij}^2)$, and $b_{ij} = -(387072/61009)(\varepsilon_{ij}/r_{s,ij}^3)$. The reduced temperature is defined as $T^* = k_B T/\varepsilon_{ff}$, where k_B is the Boltzmann constant, and the reduced density is expressed as $\rho^* = \rho\sigma_f^3$.

The FMSA is a general solution to the Ornstein-Zernike equation, with especially analytical simplicity for exponential potential function.[27,28] To extend the FMSA to LJ/s potential, we first map the potential with the two Yukawa potential, as done before by Tang an Lu[29] for the Lennard-Jones potential. With the given potential in Eq. 1, the mapping potential can be expressed by

$$u(r)^{\text{map}} = -k_1\varepsilon\frac{\exp[-z_1(r-\sigma)]}{r/\sigma} + k_2\varepsilon\frac{\exp[-z_2(r-\sigma)]}{r/\sigma} \quad (2)$$

where k_1, k_2, z_1, amd z_2 are the mapping parameters, and the values are given by $k_1 = 7.7481$, $k_2 = 7.7952$, $z_1 = 5.8690$, and $z_2 = 8.8010$. The reproduction was tested to be excellent,[24] and may be inherited in the calculation of the thermodynamic properties of LJ/s potential. In the subsequent discussion, these Yukawa potentials will substitute LJ/s potential with the mapping parameters.

FMSA with RG transformation for vapor-liquid equilibria

The reduced excess Helmholtz free energy for a fluid from the original FMSA can be usually expressed as a summation of contributions from the hard sphere repulsion and the attraction

$$a^{\text{res}} = a^{\text{rep}} + a^{\text{att}} \quad (3)$$

where the superscripts rep and att stand for hard sphere and dispersion, respectively. The hard sphere repulsion contribution is given by

$$a^{\text{rep}} = \frac{4\eta - 3\eta^2}{(1-\eta)^2} \quad (4)$$

where η is the packing factor with $\eta = \frac{1}{6}\rho\sigma^3$, and ρ is the number density of fluid. The attraction contribution can be written as[28]

$$a^{\text{att}} = 2\pi\rho\beta\int_{\sigma}^{\infty}[g(r)-1]u^{\text{map}}(r)r^2dr + 2\pi\rho\beta\int_{\sigma}^{\infty}u^{\text{LJ/s}}(r)r^2dr \quad (5)$$

where $g(r)$ can be given with the simplified exponential approximation

$$g(r) = g_0(r)\exp[g_1(r)] \quad (6)$$

$$rg_0(r) = \sum_{n=0}^{\infty}(-12\eta)^n C(1,n+1,n+1,r-n-1) \quad (7)$$

$$rg_1(r) = \beta\varepsilon k_1\frac{(1-\eta)^4}{Q^2(z_1)}\sum_{n=0}^{\infty}(1+n)(-12\eta)^n D(6,n,n+2,z_1,r-n-1) - \beta\varepsilon k_2\frac{(1-\eta)^4}{Q^2(z_2)}\sum_{n=0}^{\infty}(1+n)(-12\eta)^n D(6,n,n+2,z_2,r-n-1) \quad (8)$$

where the details of $C(n_1,n_2,n_3,r)$ and $D(n_1,n_2,n_3,z,r)$ are defined in Ref. 30. With Eq. 3, the obtained phase coexistence curve outside the critical region is believed to be reasonable. While inside the critical region, the density long-wavelength fluctuation has to be considered and FMSA, as a mean-field theory, will be inevitable to bring deviations. To remedy the deficiency, we take into account the fluctuation by general renormalization group iterations.[38–40]

$$a_n[\rho(\mathbf{r})] = a_{n-1}[\rho(\mathbf{r})] + \delta a_n[\rho(\mathbf{r})] \quad (9)$$

$$\delta a_n(\rho) = -\frac{1}{\beta V_n} \times \text{Ln}\left[\frac{\int_0^{\rho}dx\exp\{-V_n[\beta a_{n-1,D}(\rho,x) + 2\pi C_4x^2k_n^2 - 2\pi C_6x^2k_n^4]\}}{\int_0^{\rho}dx\exp\{-V_n[\beta a_{n-1,D}(\rho,x) + 2\pi C_2x^2]\}}\right] \quad (10)$$

$$a_{n-1,\text{D}}[\rho(\mathbf{r}),x] = \frac{a_{n-1}[\rho(\mathbf{r})+x] + a_{n-1}[\rho(\mathbf{r})-x]}{2} - a_{n-1}[\rho(\mathbf{r})] \quad (11)$$

$$C_n = \frac{1}{(n-1)!}\int_0^{\infty}c(r)\mathbf{r}^n d\mathbf{r} \quad (12)$$

where V_{n} is the phase space volume of n-order RG iteration, k_{n} is the fluctuation magnitude,[41] $c(r)$ is the DCF as defined in Reference 35, and the initial iteration a_0 can be calculated by Eq. 3. After several times of iteration, the excess free energy due to long-range density fluctuation is incorporated into the short-range contribution. With the total Helmholtz free energy after transformation, the global vapor-liquid diagram and critical thermodynamic properties can be calculated.

FMSA with cell model for the solid phase

To describe the thermodynamic properties of solid phase, we follow the FMSA approach similar to that for fluid phase, and assume the solid phase has a face-centered-cubic structure as described by the cell model.[35,36] The Helmholtz free energy includes a contribution from the reference hard-sphere crystal and a perturbation term by taking into account the LJ/s interaction. It writes

$$a^{\text{res}} = -\ln\left\{\frac{8}{\sqrt{2}}\left[\left(\rho\sigma^3/\sqrt{2}\right)^{1/3} - 1\right]\right\} + 12\eta\sigma^{-3}\int_{\sigma}^{\infty}g_{\text{S}}(r)u(r)^{\text{map}}dr \quad (13)$$

where $g_{\text{S}}(r)$ is the radial distribution function around an arbitrary tagged particle in crystals, and can be represented by[42]

$$g_{\text{hs}}(r) = \frac{\alpha_0}{r}e^{-\alpha_1(r-R_1)/2} + \frac{1}{24\eta}\sqrt{\alpha/2\pi} \times \sum_{i\geq 2}\frac{n_i}{rR_i}\left[-e^{\alpha(r-R_i)/2} + e^{\alpha(r+R_i)/2}\right] \quad (14)$$

in Eq. 14, n_i is the number of particles in the ith neighboring layer from the tagged particle, R_i represents the center-to-center distance between a particle in the ith layer and the tagged particle, and the determination of α_0, α_0, and R_i are given elsewhere.[42]

Fluid structure and surface tension

For the fluid in contact with a spherical particle, the system is always in equilibrium and the radius of curvature is simply varied as a boundary condition. The calculation of fluid structure and surface tension require the estimation of Helmholtz free energy. For inhomogeneous fluids, the essential task is to derive an analytical expression for the grand potential $\Omega[\rho(\mathbf{r})]$, or equivalently, the intrinsic Helmholtz free energy $a[\rho(\mathbf{r})]$ as a functional of density distribution. The grand potential $\Omega[\rho(\mathbf{r})]$ can be expressed as the following general form of density functional

$$\Omega[\rho(\mathbf{r})] = \int d\mathbf{r}\rho(\mathbf{r})\left[\ln\left(\rho(\mathbf{r})\Lambda^3\right) - 1\right] + a_{\text{rep}}[\rho(\mathbf{r})] + a_{\text{att}}[\rho(\mathbf{r})] + \int d\mathbf{r}[\rho(\mathbf{r})(V_{\text{ext}}(\mathbf{r}) - \mu)] \quad (15)$$

where $\rho(\mathbf{r})$ denotes the density distribution with configuration $\mathbf{r}$, $a_{\text{rep}}[\rho(\mathbf{r})]$ stands for the hard-sphere reference system, $a_{\text{att}}[\rho(\mathbf{r})]$ accounts for the attractive interactions, μ represents the chemical potential in the ensemble, and $V_{\text{ext}}(\mathbf{r})$ is the external potential for the fluid-nanoparticle interaction, as given by Eq. 1.

The hard-sphere functional can be well described by MFMT,[25,26] which gives more accurate density profiles in a number of inhomogeneous systems. It writes

$$a_{\text{rep}}[\rho(\mathbf{r})] = \int d\mathbf{r}\left[-n_0\ln(1-n_3) + \frac{n_1n_2 - \mathbf{n_{v1}}\mathbf{n_{v_2}}}{1-n_3} + \frac{1}{36\pi}\left(n_3\ln(1-n_3) + \frac{n_3^2}{(1-n_3)^2}\right)\frac{n_2^3 - 3n_2\mathbf{n_{v1}}\mathbf{n_{v2}}}{n_3^3}\right] \quad (16)$$

where $n_\alpha(\mathbf{r})$, $\alpha = 0,1,2,3,\mathbf{V}1,\mathbf{V}2$ are the scalar and vector weighted densities from the fundamental measure theory.[43]

For the attractive part, the explicit analytical direct correlation function (DCF) from the FMSA provides an accurate description for curved surface

$$a_{\text{att}}[\rho(\mathbf{r})] = a_{\text{att}}(\rho_{\text{b}}) + \mu\int\frac{\mathbf{r_1}}{\mathbf{r}}\Delta\rho(\mathbf{r}_1)\,d\mathbf{r}_1 - \frac{1}{2}\int\frac{\mathbf{r_1}}{\mathbf{r}}\Delta\rho(\mathbf{r}_1)d\mathbf{r}_1\int\frac{\mathbf{r_2}}{\mathbf{r_1}}c(\mathbf{r}_1-\mathbf{r}_2)\Delta\rho(\mathbf{r}_2)d\mathbf{r}_2 \quad (17)$$

where the subscript "b" represents the bulk fluid, or the equilibrated fluid, and $\Delta\rho(\mathbf{r}) = \rho(\mathbf{r}) - \rho_{\text{b}}$. The reliable bulk physical properties can be given by the FMSA outside the critical region, and by the FMSA with RG transformation inside the critical region. With the above expression for the intrinsic Helmholtz free energy, the density distribution can be obtained by minimizing the grand potential

$$\rho(\mathbf{r}) = \rho_{\text{b}}\exp\left(\beta\mu_{\text{b,ex}} - \beta\frac{\delta\left(a_{\text{rep}}[\rho(\mathbf{r})] + a_{\text{att}}[\rho(\mathbf{r})]\right)}{\delta\rho(\mathbf{r})} - \beta V_{\text{ext}}(\mathbf{r})\right) \quad (18)$$

Equation 18 can be calculated by use of Picard iteration,[44] and the iterations terminate when the maximum difference between two subsequent density profiles is smaller than 10^{-6}.

With the obtained density profile, the grand potential can be obtained by Eq. 15. The surface tension γ_{s} can be calculated with the grand potential and the saturation pressure of fluid (P)

$$\gamma_{\text{s}} = \frac{\Omega + PV}{A} \quad (19)$$

Here A is the surface area. For curved surface, it writes

$$\gamma_{\text{s}} = \int_R^\infty\left(\frac{r}{R}\right)^2[a[\rho(r)] - \rho(r)\mu + \rho(r)V_{\text{ext}}(r) + P]dr \quad (20)$$

Line tension and modified Young's equation

Young's equation provides a simple description of wetting and drying transitions in terms of the surface tensions of the different interfaces. These transitions have been studied extensively to evaluate the contact angle for fluid-wall systems with the vapor-wall γ_{vw} and liquid-wall γ_{lw} surface tension[45]

$$\cos\theta = \frac{\gamma_{\text{vw}} - \gamma_{\text{lw}}}{\gamma_{\text{vl}}} \quad (21)$$

This expression is called as the Young's equation, which is very accurate for fluid-wall system. It is known that the Young's equation fails to some systems, where the line tension has a considerable influence on the wetting transition, and therefore it has to be considered as a correction in a more general treatment.[11] The corresponding modified Young equation is

$$\gamma_{\text{pv}} - \gamma_{\text{pl}} - \gamma_{\text{lv}}\cos\theta + \frac{\tau\cos\theta}{R\sin\theta} = 0 \quad (22)$$

where γ_{pv}, γ_{pl}, and γ_{lv} denote the surface tension of the vapor-particle, liquid-particle and vapor-liquid interface respectively, τ represents the line tension and defined as the excess energy that is associated with the three-phase line, and θ is the modified contact angle between liquid and particle. Following Marmur's analysis,[14,15] the line tension can be defined as the difference per unit length of the contact line l_{plv} between the actual interfacial energy U_{plv} of the system and the independent interfacial energy, which is calculated based on the assumption that there is no effect on the surface tensions between any two phases from the third phase

$$\tau l_{\text{plv}} \equiv U_{\text{plv}} - (U'_{\text{lv}} + U'_{\text{pv}} + U'_{\text{pl}}) \quad (23)$$

where U_{plv} is the sum of all molecular interactions, $U'_{i,j}$ is the independent interfacial energy between phases i and j,

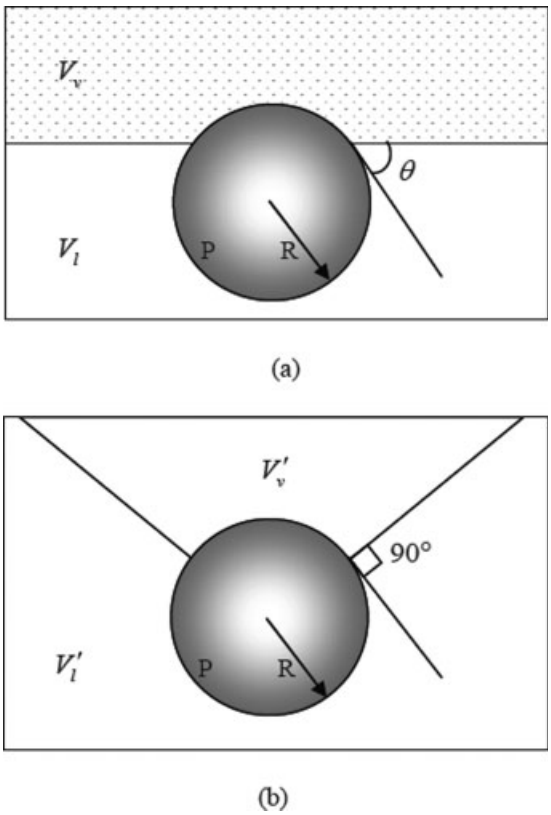

Figure 2. The geometrical definitions of integral regions for different interfacial energy calculation.

(a) Actual interfacial energy, (b) independent interfacial energy.

l_{plv} is the length of the contact line and can be denoted with the radius R of the particle and the contact angle by

$$l_{plv} = 2\pi R \sin\theta \tag{24}$$

However, as discussed in the introduction, each interfacial tension in a wetting system is affected to some extent by the presence of the third phase; this is particularly true in the close vicinity of the contact line. To derive the line tension, we assume the actual total interfacial energy of the system can also be divided to three dependent terms, each of which is affected by a nearby third phase

$$U_{plv} = U_{lv} + U_{pv} + U_{pl} \tag{25}$$

For the specific case of a vapor-liquid-particle system, the difference between the vapor-liquid interfacial energy with or without the effect of the third phase is very small, and can be neglected for simplicity. Then, Eq. 23 is revised to

$$\tau l_{plv} \equiv U_{pv} + U_{p1} - (U'_{pv} + U'_{pl}) \tag{26}$$

Furthermore, we find that the total and independent vapor-particle and liquid-particle energies can be calculated within different integral regions as shown in Figure 2. Thus, they can be expressed with

$$U_{pv} + U_{pl} = \int_{V_v} V_{ext}(\mathbf{r})\rho_v(\mathbf{r})d\mathbf{r} + \int_{V_l} V_{ext}(\mathbf{r})\rho_l(\mathbf{r})d\mathbf{r} \tag{27}$$

and

$$U'_{pv} + U'_{pl} = \int_{V'_v} V_{ext}(\mathbf{r})\rho_v(\mathbf{r})d\mathbf{r} + \int_{V'_l} V_{ext}(\mathbf{r})\rho_l(\mathbf{r})d\mathbf{r} \tag{28}$$

where V_v, V_l, V'_v, and V'_l are corresponding integral regions. If we use Eqs. 26–28 to calculate the line tension directly, the accumulative error from those integrals may be considerable. To avoid error accumulation, Eq. 26 can be transformed into a derivative form

$$\frac{d\tau}{dR} l_{plv} + \frac{dl_{plv}}{dR}\tau \approx \frac{dU_{pv}}{dR} + \frac{dU_{pl}}{dR} - \left(\frac{dU'_{pv}}{dR} + \frac{dU'_{pl}}{dR}\right) \tag{29}$$

and τ can be further expended to

$$\tau(R_1) = \tau(R_0) + \frac{d\tau}{dR_0}(R_1 - R_0) + \cdots \tag{30}$$

where the high order terms are neglected. Combining Eqs. 29, 30 with Eq. 22, we can solve τ, cos θ, and $\frac{d\tau}{dR}$ simultaneously by a simply Picard iteration method[44] with $\Delta R = 0.0025\sigma_f$. The solution indicates that the line tension depends not only on the contact angle, but also on the curvature of the particle surface.

Results and Discussion

To calculate the wetting angle of nanoparticle at the equilibrated vapor-1iquid interface, the independent surface tensions should be obtained in advance. However, surface tension calculation needs the equilibrium properties of fluids as input. As a result, we begin our discussion with the phase behavior.

Global vapor-liquid-solid phase diagram

We first predicted the global vapor-liquid phase behavior for LJ/s fluids using the FMSA with RG transformation (FMSA+RG), and compared with molecular simulation data[46,47] to validate its predictive ability. The results are shown in Figure 3, in which those from the original FMSA are also given for comparison. Outside the critical region, the original FMSA behaves similar to the FMSA+RG; whereas inside the critical region, FMSA overestimates liquid densities and underestimates vapor densities. The FMSA+RG, however, reproduces quite well the molecular simulation results. As pointed out before, the original FMSA remains to be a mean-field type, in which the long-range density fluctuation inside the critical region cannot be considered. Evidently, it overestimates the critical point as well as the surrounding region. In contrast, the FMSA+RG, by considering the inhomogeneity and the long-range density fluctuations of

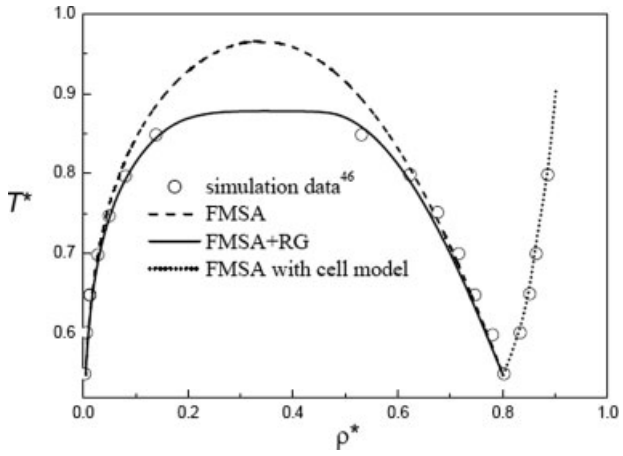

Figure 3. The global vapor-liquid-solid equilibria of LJ/s fluids.

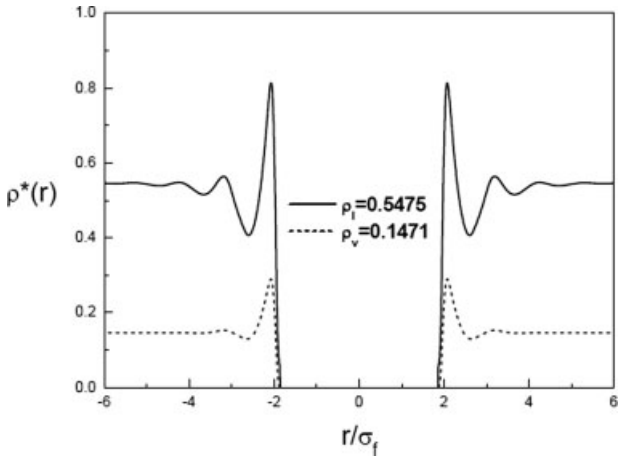

Figure 4. Calculated local density profiles of fluid around a nanoparticle with $\sigma_p = 3\sigma_f$ in critical region ($T^* = 0.85$).

Solid lines correspond to equilibrium liquid; dash lines correspond to equilibrium vapor phase.

fluids, is capable of predicting the critical properties correctly.

On the other hand, it is very difficult for molecular simulation to calculate the properties in the vicinity of the critical point because of the large density fluctuation. The critical temperature, pressure and density are commonly estimated by fitting the subcritical coexisting data. For example, the critical temperature estimated by Røsjorde et al.,[46] is 0.897 in reduced units, whereas by Bresme[47] the value is 0.91. The theoretical model, however, can predict criticality in consistence with the global phase behavior. In this work, the critical temperature theoretically calculated is 0.879. Although the true value is unknown, it seems that the theoretical value is more reasonable by fully evaluating Figure 3. The figure indicates that the FMSA+RG can accurately describe the global vapor-liquid phase behavior in a simple and flexible way.

To give a global phase description for LJ/s fluids, Figure 3 also shows the fluid-solid transition predicted by the FMSA combined with the cell model. In this case, the phase diagram includes a triple point where vapor, liquid, and solid are in equilibrium. Obviously, the calculated freezing line is in good agreement with simulation results[46]; this demonstrates that the FMSA can also be extended to solid phase.

The structure of fluid and independent surface tension

As well addressed before,[24] our density functional method can predict the fluid structure accurately. Especially, with the RG transform, the method has the advantage over other traditional density functional theories in the description of critical region of fluids. Even compared with molecular simulation, the feature in critical property calculation makes the model have strong advantage. Figure 4 shows the density profiles for fluid around a nanoparticle, where the liquid is in equilibrium with the coexisting vapor. The size of nanoparticle is $\sigma_p = 3\sigma_f$, and the reduced temperature is $T^* = 0.85$, very close to the critical point. From the figure one can see that the oscillating density in the liquid-particle interface is caused by the repulsive force, and the impact of the attractive force from the particle on the structure of the liquid extends over $5\sigma_f$; this indicates that nanoscale contact problem cannot be ignored in the Young's equation.[21]

With the accurate fluid structure, the chemical potential, Helmholtz free energy, and grand potential were obtained using our model. Accordingly, the independent vapor-liquid, vapor-nanoparticle, and liquid-nanoparticle surface tensions were calculated. It is well known that the accurate vapor-liquid surface tension can be easily predicted by a variety of density functional methods. Thus, only the vapor-nanoparticle and liquid-nanoparticle surface tensions were discussed in this work. Figure 5 shows the two surface tensions as a function of the inverse of particulate size with strong fluid-nanoparticle interactions ($\varepsilon_{pf} = 1.75\varepsilon_{ff}$), as well as the results from molecular simulations.[45] For the vapor-nanoparticle part, the agreement is excellent; while for the liquid-nanoparticle part, it shows slight deviations from the simulation

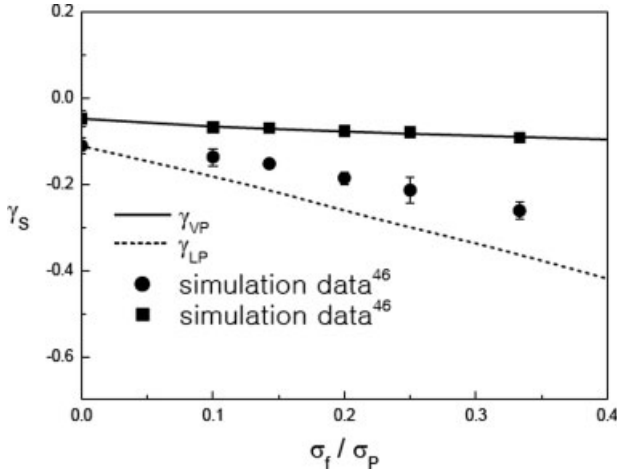

Figure 5. Comparison of vapor-nanoparticle and liquid-nanaparticle surface tensions for $\varepsilon_{pf} = 1.75\varepsilon_{ff}$ and $T^* = 0.75$.

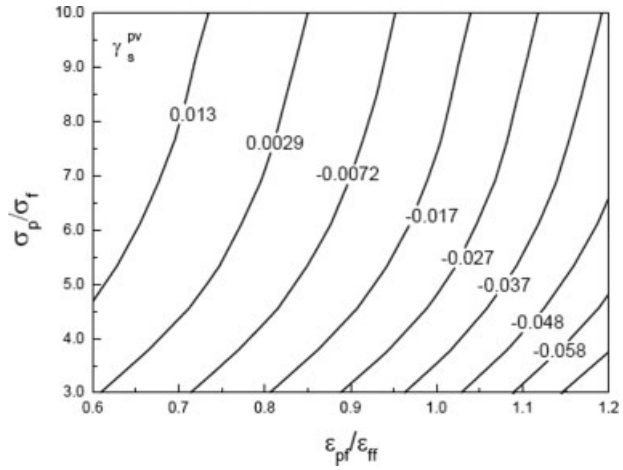

Figure 6. The calculated contour lines of vapor-nanoparticle surface tension with size ratio on the ordinate and energy ratio on the abscissa (T^* = 0.85).

data,[45] and the deviation increases with decreasing nanoparticle size. The deviation may be attributed to two aspects: the inaccurate interfacial energy calculation in the theoretical model is due to the strong density oscillation at the interface, and the uncertainty in molecular simulations is due to the complexity of the system. Nevertheless, the predicted liquid-particle surface tension is still reasonable. These comparisons show that our method is a good approach to calculate independent surface tensions.

Further predictions of independent vapor-nanoparticle and liquid-nanoparticle surface tensions in the critical region (T^* = 0.85) were performed. Figures 6 and 7 show the contour lines of vapor-nanoparticle and liquid-nanoparticle surface tensions, respectively. From the two figures, one can find that, if the strength of fluid-nanoparticle interactions increases, or the nanoparticle size decreases, the surface tensions can be changed from positive to negative. Generally speaking, negative surface tensions can be interpreted in principle as a tendency of the nanoparticle to disperse in the fluid.[45] Therefore, decreasing the nanoparticle size and increasing the fluid-nanoparticle interaction energy are favorable to the dispersion of nanoparticles in fluid.

Line tension and the modified contact angle

With the independent vapor-liquid, vapor-particle, and liquid-particle surface tensions as input, the calculated contact angles by the Young's and the modified Young's equations as a function of the fluid-particle interaction strength for $\sigma_p = 5\sigma_f$ and $\sigma_p = 10\sigma_f$ are given in Figure 8. One thing should be highlighted is that, in the modified Young's equation, free energy was included in the line tensions for three-phase contact. It seems that the contact angles obtained by the Young's and the modified Young's equations are all in good agreement with the simulation data,[11] and the two equations yield nearly undistinguishable curves. The results demonstrate that, from another point of view, the three independent surface tensions calculated with our theoretical model are reliable. The unobvious modification of contact angles reveals that the line tension is very small, and the Young's equation is still suitable for large nanoparticles. Figure 8 also shows that, for a given interaction strength, an increase in size of the nanoparticle produces an increase in the contact angle.

To give insight into the effect of the curvature of the nanoparticle, the contact angles for smaller nanoparticles were further investigated. Figure 9 depicts the calculated contact angles as a function of the nanoparticle size. For comparison, the two molecular dynamic simulation results, by direct measurement of the contact angle and by the excess three-phase contact energy calculation respectively, are also given. The results for the contact angles obtained from the theory and the two simulation methods agree well for nanoparticles larger than $5\sigma_f$. In this case, both the Young's and the modified Young's equations are valid. However, for smaller nanoparticles, the deviation between the two simula-

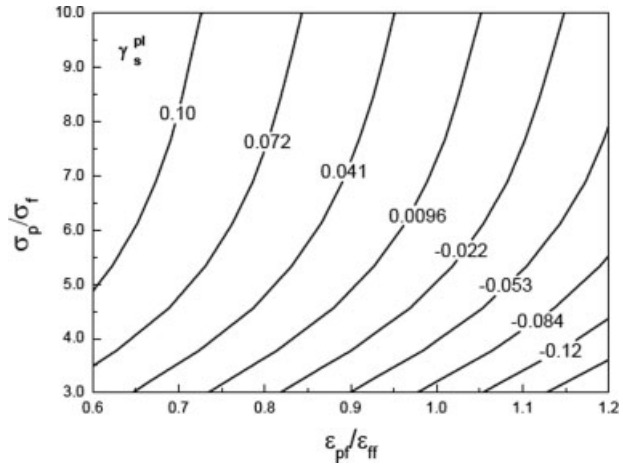

Figure 7. The calculated contour lines of liquid-nanoparticle surface tension with size ratio on the ordinate and energy ratio on the abscissa (T^* = 0.85).

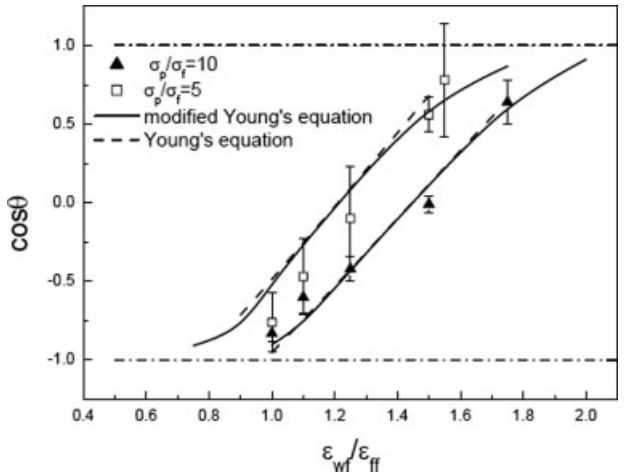

Figure 8. Comparison of the predicted contact angles by the theoretical model, molecular simulation,[11] the Young's and the modified Young's equations with T^* = 0.75.

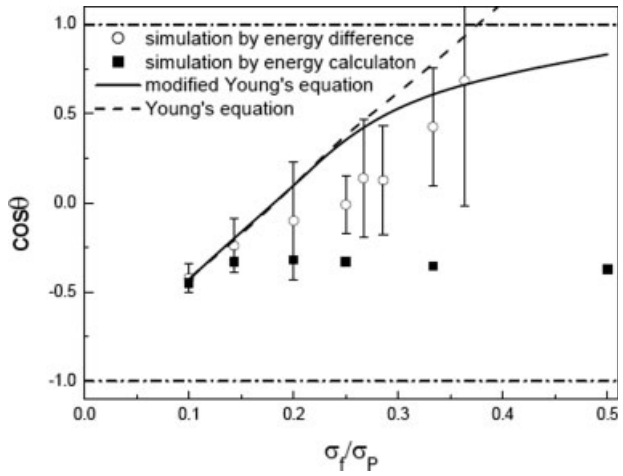

Figure 9. Comparison of the contact angles by the theoretical model, molecular simulation,[11] the Young's and the modified Young's equations as a function of the nanoparticle size with $\varepsilon_{pf} = 1.25\varepsilon_{ff}$ and $T^* = 0.75$.

tion results becomes obvious. We think that, for molecular simulation, the direct observation results are more reasonable because the energy route includes some assumptions and can easily bring accumulative error. On the other hand, the modified contact angles obtained by considering the line tension in our theoretical model are similar to the values from direct measurement of contact angle simulations.[11] Figure 10 shows the estimates of the line tension, which are also comparable to the simulation results.[11] These results validate our line tension derivation and calculation based on the independent vapor-liquid, vapor-particle, and liquid-particle interfacial tensions. If the line tension factor is neglected, the contact angles yielded by the Young's equation shown in Figure 9 become worse with the decrease of the nanoparticle size. The deterioration could be more serious in stronger fluid-nanoparticle interaction region at higher temperature. On the other hand, Figure 10 also indicates that the shift in the angle is consistent with the line tension sign.

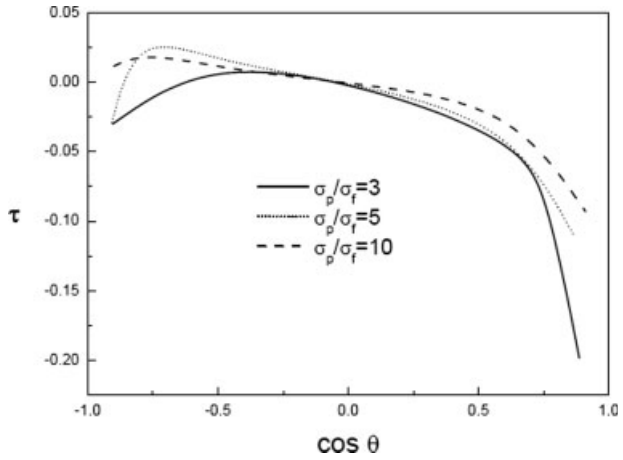

Figure 10. The calculated line tensions as a function of contact angle (cos θ) with $T^* = 0.75$.

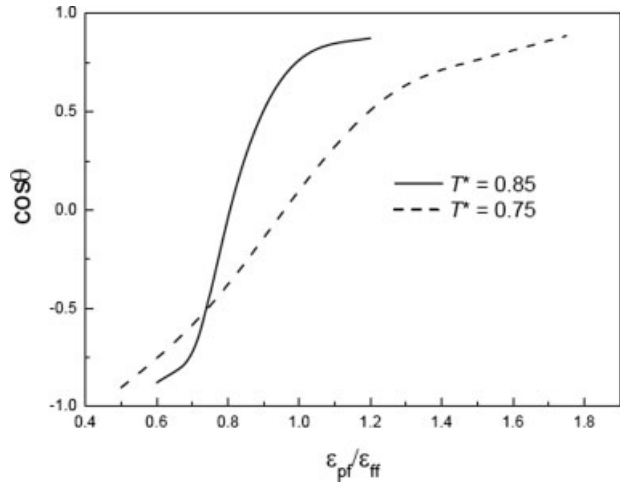

Figure 11. Influences of the fluid-nanoparticle interaction strength on the contact angle (cos θ) at different fluid temperatures.

Further investigation was performed to evaluate the influence of fluid temperature, especially in the critical region. Figure 11 plots the modified contact angle as a function of the interaction strength for $\sigma_p = 3\sigma_f$ with T* = 0.75 and T* = 0.85, respectively. As expected, the influence of interaction strength on wetting transition increases with increasing temperature. The results suggest that, outside the critical region, the wetting transition tends toward the first order, whereas inside the critical region, it tends toward the second order, similar to the fluid phase transition.

Conclusions

In this work, a theoretical model was developed based on density functional method to deal with the wetting behavior of nanoparticles at fluid interface. Particularly, a new method for line tension calculation was derived. In this model, the FMSA theory, the RG transformation, the cell model, and the MFMT are integrated. As our RG transformation was constructed with the same background of the FMSA, the whole theoretical framework is rigorous and consistent.

The predictive capability of the model for global vapor-liquid-solid phase equilibria of LJ/s fluids was discussed. With the accurate equilibrated densities, the structures of fluid around the nanoparticles were calculated, and the independent vapor-liquid, vapor-nanoparticle, and liquid-nanoparticle surface tensions were obtained. Comparisons with molecular simulation data show that the vapor-liquid and vapor-nanoparitcle surface tensions are accurate, and the liquid-nanoparticle results are also reliable.

The new line tension calculation method was extended to analyze the wetting angle and to revise the Young's equation, and the results were validated with molecular simulation data. The present work shows that the line tension has large influence on wetting properties for small nanoparticles; whereas for large nanoparticles, the effect is negligible. In summary, this work presents a theoretical model that can deal with the global three-phase behavior, interfacial surface tensions, the line tension of the three-phase contact, as well

as the contact angle simultaneously for nanoparticles at fluid interfaces.

Acknowledgments

The financial support of the NSFC (20576006, 20676004, 20876007) is greatly appreciated.

Literature Cited

1. Edwards DA, Brenner H, Wasan, DT. *Interfacial Transport Processes and Rheology*. Boston: Butterworth-Heinemann, 1991.
2. Griffiths JA, Bolton R, Heyes DM, Clint JH, Taylor SE. Physicochemical characterisation of oil-soluble overbased phenate detergents. *J Chem Soc Faraday Trans*. 1995;91:687–696.
3. Bresme F, Oettel M. Nanoparticles at fluid interfaces. *J Phys: Condens Matter*. 2007;19:413101.
4. Bowden N, Terfort A, Carbeck J, Whitesides GM. Self-assembly of mesoscale objects into ordered two-dimensional arrays. *Science*. 1997;276:233–235.
5. Rowlinson JS, Widom B. *Molecular Theory of Capillarity*. New York: Oxford Science Publications, 1989.
6. Rowlinson JS, Widom B. *Molecular Theory of Capillarity*. New York: Dover, 2002.
7. Verdaguer A, Sacha GM, Bluhm H. Salmeron M. Molecular structure of water at interfaces: wetting at the nanometer scale. *Chem Rev*. 2006;106:1478.
8. Aveyard R, Clint JH, Nees D. Theory for the determination of line tension from capillary condensation. *J Chem Soc Faraday Trans*. 1997;93:4409–4411.
9. Tay KA, Bresme F. Wetting properties of passivated metal nanocrystals at liquid-vapor interfaces: a computer simulation study. *J Am Chem Soc*. 2006;128:14166–14175.
10. Amirfazli A, Neumann AW. Status of the three-phase line tension: a review. *Adv Colloid Interface Sci*. 2004;110:121–141.
11. Bresme F, Quirke N. Computer simulation of the wetting behavior and line tensions of nanometer size particulates at a liquid-vapor interface. *Phys Rev lett*. 1998;80:3791–3794.
12. Bresme F, Quirke N. Nanoparticulates at liquid/liquid interfaces. *Phys Chem Chem Phys*. 1999;1:2149–2155.
13. Faraudo J, Bresme F. Stability of particles adsorbed at liquid/fluid interface: shape effects induced by line tension. *J Chem Phys*. 2003;118:6518–6528.
14. Marmur A. Line tension and the intrinsic contact angle in solid-fluid-fluid systems. *J Colloid Interface Sci*. 1997;186:462–466.
15. Marmur A, Krasovitski B. Line tension on curved surface: liquid drops on solid micro- and nanospheres. *Langmuir*. 2002;18:8919–8923.
16. Djikaev Y, Widom B. Geometric vier of the thermodynamics of adsorption at a line of three-phase contact. *J Chem Phys*. 2004; 121:5602–5610.
17. Widom B. Models of adsorption at a line of three-phase contact. *J Phys Chem B*. 2006;110:22125–22132.
18. Schimmele L, Napiórkowski M. Conceptual aspects of line tension. *J Chem Phys*. 2007;127:164715.
19. Napari I, Laaksonen A. The effect of potential truncation on the gas-liquid surface tension of planar interfaces and droplets. *J Chem Phys*. 2001;114:5796–5801.
20. Moody MP, Attard P. Monte Carlo simulation methodology of the ghost interface theory for the planar surface tension. *J Chem Phys*. 2004;120:1892–1904.
21. Ingebrigtsen T, Toxvaerd S. Contact angles of lennard-jones liquids and droplets on planar surfaces. *J Phys Chem C*. 2007;111:8518–8523.
22. Santiso E, Firoozabadi A. Curvature dependency of surface tension in multicomponent systems. *AIChE J*. 2006;52:311–322.
23. Tolman RC. The effect of droplet size on surface tension. *J Chem Phys*. 1949;17:333–337.
24. He Y, Mi J, Zhong C. Surface tension and Tolman length of spherical particulate in contact with fluid. *J Phys Chem B*. 2008;112: 7251–7256.
25. Yu YX, Wu J. A fundamental-measure theory for inhomogeneous associating fluids. *J Chem Phys*. 2002;116:7094–7103.
26. Yu YX, Wu J. Structures of hard-sphere fluids from a modified fundamental-measure theory. *J Chem Phys*. 2002;117:10156–10164.
27. Tang YP, Lu BCY. A new solution of the Ornstein-Zernike equation from the perturbation theory. *J Chem Phys*. 1993;99:9828–9835.
28. Tang YP, Tong Z, Lu BCY. Analytical equation of state based on the Ornstein-Zernike equation. *Fluid Phase Equilib*. 1997;134:21–42.
29. Tang YP, Lu BCY. Analytical description of the Lennard-Jones fluid and its application. *AIChE J*. 1997;43:2215–2226.
30. Tang YP, Wu J. Modeling inhomogeneous van der Waals fluids using an analytical direct correlation function. *Phys Rev E*. 2004;70: 011201.
31. Tang YP. First-order mean spherical approximation for inhomogeneous fluids. *J Chem Phys*. 2004;121:10605–10610.
32. Mi J, Zhong C, Li YG, Tang YP. Prediction of global VLE for mixtures with improved renormalization group theory. *AIChE J*. 2006; 52:342–353.
33. Mi J, Tang YP, Zhong C. Li YG. Prediction of global vapor-liquid equilibria for mixtures containing polar and associating components with improved renormalization group theory. *J Phys Chem B*. 2005; 109:20546–20553.
34. Mi J, Tang YP, Zhong C. Theoretical study of Sutherland fluids with long-range, short-range, and highly short-range potential parameters. *J Chem Phys*. 2008;128:054503.
35. Wu J, Prausnitz JM, Hu Z. Crystalline and liquid-crystalline properties of polyesters of phenyl-substituted 4,4′-biphenol. I. Polymers from terephthalic acid and 2,6-naphthalenedicarboxylic acid. *Macromolecules*. 2003;36:440–446.
36. Fu D, Li YG. Effect of the range of attractive interactions on crystallization, metastable phase transition, and percolation in colloid dispersion. *Phys Rev E*. 2003;68:011403.
37. Hoover BL. *Computational Statistical Mechanics*. Amsterdam: Elsevier, 1991.
38. Wilson KG. Renormalization group and critical phenomena. I. Renormalization group and the Kadanoff scaling picture. *Phys Rev B*. 1971;4:3174–3183.
39. Wilson KG. Renormalization group and critical phenomena. II. Phase-space cell analysis of critical behavior. *Phys Rev B*. 1971;4: 3184–3205.
40. White JA, Zhang S. Renormalization group theory for fluids. *J Chem Phys*. 1993;99:2013–2019.
41. Nijmeijer MJP, Bruin C, Bakker AF, van Leeuwen JMJ. Wetting and drying of an inert wall by a fluid in a molecular-dynamics simulation. *Phys Rev A*. 1990;42:6052–6059.
42. Rascón C, Mederos L, Navascuıs G. Theoretical approach to the correlations of a classical crystal. *Phys Rev E*. 1996;54:1261–1264.
43. Rosenfeld Y. Free energy model for the inhomogeneous hard-sphere fluid mixture and density-functional theory of freezing. *Phys Rev Lett*. 1989;63:980–983.
44. Hansen JP, McDonald IR. *Theory of Simple Liquids[M]*, 2nd ed. London: Academic, 1986.
45. Bresme F, Quirke N. Computer simulation of wetting and drying of spherical particulates at a liquid-vapor interface. *J Chem Phys*. 1999; 110:3536–3547.
46. Røsjorde A, Fossmo DW, Bedeaux D, Kjelstrup S, Hafskjold B. Nonequilibrium molecular dynamics simulations of steady-state heat and mass transport in condensation I. local equilibrium. *J Colloid Interface Sci*. 200;232:178–185.
47. Bresme F. Integral equation study of the surface tension of colloidal-fluid spherical interfaces. *J Phys Chem B*. 2002;106:7852–7859.
48. Nijmeijer MJP, Bruin C, Bakker AF, van Leeuwen JMJ. Determination of the location and order of the drying transition with a molecular-dynamics simulation. *Phys Rev B*. 1991;44:834–837.

Manuscript received Jun. 6, 2008, and revision received Sept. 9, 2008.